Dynamic Behavior of Plasma in a Cascade Plasma Torch with External Magnetic Field

Hiroki Saito[1] · Hikaru Matsumoto[1] · Takayasu Fujino[1]

Abstract The effect of operating conditions on the arc voltage fluctuations and dynamic behavior of plasma were investigated for a cascade plasma torch with an external magnetic field. The key factors that affect the fluctuations of the arc voltage were studied, which is useful for generating stable plasma jets. A ring-shaped permanent magnet was used to produce an external magnetic field having a flux density of approximately 0.27 T at the center of the magnet. The operating current, gas flow rate, and anode–cathode distance were varied in the range of 40-160 A, 10-40 L/min, and 0-10 mm, respectively. The width of the ring-shaped anode was set to 1 mm or 3 mm. The end-on images of the plasma were captured by high-speed photography, and the associated arc voltage was measured simultaneously. When an anode of 1 mm width was used, a periodic sine-like voltage waveform with low amplitude was observed at a low gas flow rate. In that condition, an arc root rotated along the anode wall continuously with no observable breakdown process. The rotational frequencies of the arc exceeded 1 kHz and were strongly dependent on the square root of the operating current.

✉ Hiroki Saito
hiroki.saito@rift.mech.tohoku.ac.jp

Takayasu Fujino
tfujino@kz.tsukuba.ac.jp

1 Department of Engineering Mechanics and Energy, University of Tsukuba, 1-1-1 Tennodai, Tsukuba, Ibaraki 305-8577, Japan

Introduction

In atmospheric plasma spraying processes, it is known that arc fluctuations (Ref 1) in a non-transferred dc plasma torch affect the plasma jet properties (Ref 2–5), heat and momentum transfers to particles (Ref 6), and final coating structures (Ref 7). When the arc slides or jumps in the plasma torch, the time variation of input power occurs due to the change in the arc resistance (Ref 8–10). Although the motion of the arc is necessary to limit the anode erosion, the suppression of arc fluctuations is an important strategy improving the reproductivity and controllability of coating properties.

One of the effective methods to suppress arc fluctuations is the use of a cascade plasma torch (Ref 11, 12). The cascade plasma torch consists of a rod-type cathode, ring-shaped anode, and stack of neutral insulators. The neutral insulators are placed intermediately between the anode and cathode to stabilize the time-averaged arc length and limit the arc movement in the flow direction. This approach involving the cascade electrode has been employed, for example, in the Triplex plasma torch (Ref 13). It is reported that this torch generates stable plasma jets with low voltage fluctuations (Ref 14). The cascade plasma torch also allows for adjustment of the time-averaged arc voltage by changing the number of neutral insulators.

Recently, it has also been reported that applying an external magnetic field to the plasma torch (Ref 15) could improve the arc voltage stability (Ref 16, 17). The interaction between the anode arc current and external magnetic

field in the flow direction produces Lorentz force in the circumferential direction. Using this force, the anode arc root is forcibly rotated in the plasma torch. This rotation is expected to contribute to the improvement in the controllability of the dynamic behavior of the arc in the torch as well as the limit of electrode erosion (Ref 18). However, whether the application of the external magnetic field reduces the arc voltage fluctuations depends strongly on the operating conditions of the torch (Ref 16, 17, 19, 20).

By combining these two methods, there is a possibility of designing a plasma torch with low arc voltage fluctuations. The time-averaged voltage in the plasma torch may be controlled by the use of a cascade electrode, and longer anode lifetime may be obtained by the use of an external magnetic field. In this study, a cascade plasma torch with a permanent magnet was constructed. Although the input power of the constructed plasma torch was smaller than that of a practical plasma torch for thermal spraying, most of the same basic phenomena of arc dynamics were observed in the experiment. The analysis of this experimental torch will help to improve understanding of the key factors which affect the arc voltage fluctuations. The effects of using a cascade electrode and applying an external magnetic field on the voltage–current characteristics were investigated. Besides, the effects of the gas flow rates and anode width on the arc voltage fluctuations and dynamic behavior of the plasma were studied to reveal the appropriate operating conditions for generating plasma jets with low power fluctuations. The arc rotational frequency for different operating currents was also the part of the investigation.
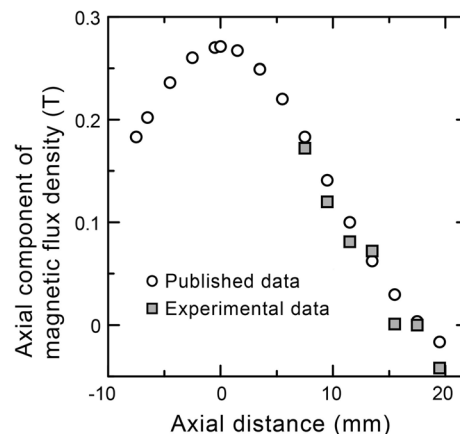
Experimental Setup

The experimental setup mainly consists of a few kW dc power sources, a non-transferred dc plasma torch, a gas supply system, an observation system of plasma jets, and a voltage–current measurement and record system. A power source for TIG (tungsten inert gas) welding (Panasonic YC-200BR1) was used to generate the plasma. A passive high-voltage probe (Yokogawa 700929, dc-100 MHz) and a Hall effect current sensor (U_RD HCS-20-100-AS, dc-20 kHz) were used for the voltage and current measurements, respectively. The output signals from the probe and the sensor were recorded using a high-speed data acquisition unit (Yokogawa SL1000 with the module 720210, dc-20 MHz). The end-on images of the plasma jets were captured by the high-speed camera (nac MEMRECAM HX-3).

Figure 1 shows the schematic of the non-transferred dc plasma torch. The cascade electrode consists of a rod-type cathode, water-cooled ring-shaped anode, and stack of

cylindrical insulators. The cathode (2.4 mm in diameter) and anode (6.5 mm in inner diameter) are made of tungsten with the addition of 2% cerium and oxygen-free copper, respectively. The positions of the ring-shaped anode and insulators are interchangeable. The horizontal distance from the cathode tip to the upstream side of the anode is defined as the anode–cathode distance. A ring-shaped NdFeB permanent magnet (NeoMag, N40) is placed around the plasma torch to apply an external magnetic field. The thickness of the magnet is 15 mm, and the inner and outer diameters of the magnet are 32 mm and 70 mm, respectively. The axial component of the magnetic flux density along the axis of the magnet was measured from the top side of the magnet using a Gauss meter (Toyo Lakeshore421). Figure 2 shows the comparison of the magnetic field between the published data (Ref 21) and experimentally measured data. The axial distances of 0 mm and 7.5 mm correspond to the center and top side of the magnet, respectively. The published data and
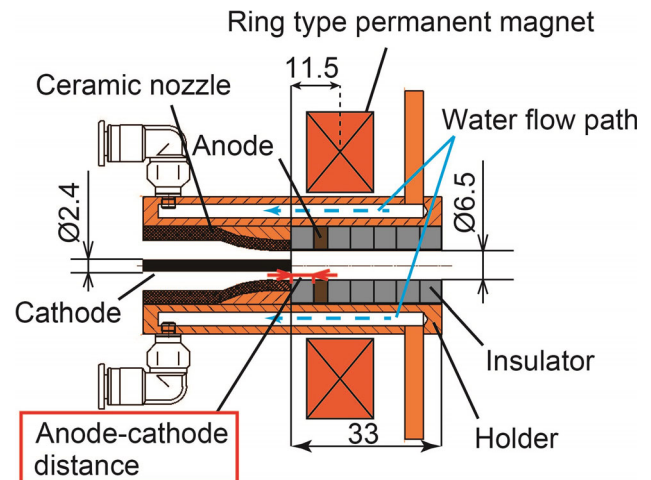
Fig. 1 Schematic diagram of the plasma torch

Fig. 2 Distribution of axial component of magnetic flux density

experimental data agree well with respect to the magnitude over the range from 7.5 to 20 mm. In the published data, the magnetic field takes the maximum value of approximately 0.27 T at the center of the magnet.

Table 1 summarizes the experimental conditions. Pure argon was used as the working gas. The operating current, gas flow rate, and anode–cathode distance were varied in the ranges of 40-160 A, 10-40 L/min, and 0-10 mm, respectively. The width of the anode used in the experiment was 1 mm or 3 mm. The voltage was recorded for 100 ms after an arbitrary interval from the plasma ignition, and the end-on images of the plasma jets were captured using high-speed photography. The high-speed camera was placed at a distance of approximately 0.5 m from the plasma torch outlet. To reduce the light intensity from the plasma and zoom in on the plasma jets, a neutral density filter and tele-conversion lens were used. The exposure time, frame rates, and image resolution were set to 0.2 μs, 100,000 fps, and 192 × 200 pixels, respectively. The experiment was performed three times for each operating condition at atmospheric pressure.

Results and Discussion

Voltage–Current Characteristics

When the anode–cathode distance was set to 10 mm, no plasma ignition was observed. The results corresponding to the anode–cathode distances of 0 mm and 5 mm are discussed below. Figure 3 shows the voltage–current characteristics of the cascade plasma torch with no external magnetic field. The gas flow rate and anode width were set to 20 L/min and 3 mm, respectively. The results for a normal plasma torch, having a normal cylindrical anode and no insulators, are also shown in Fig. 3 for the purpose of comparison. The vertical bars represent the averaged standard deviation of three measurements for each operating current condition. The voltage–current curves show a
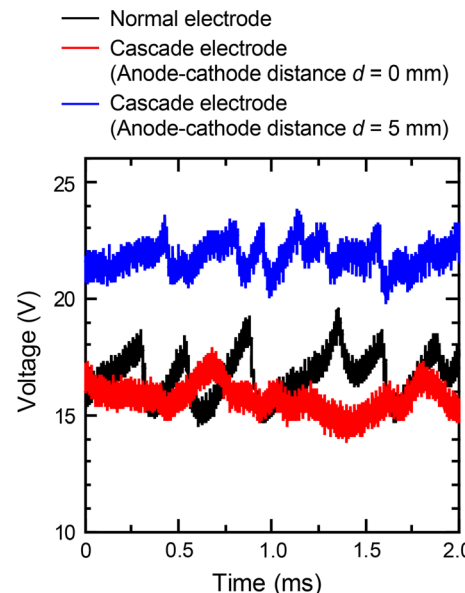
typical negative trend regardless of the electrode types. As the operating current increases, the input power, which is simply calculated as the product of the voltage and operating current, also rises for each electrode type. When a cascade electrode is used, higher time-averaged voltages are obtained by increasing the anode–cathode distance. This may be attributed to a longer arc elongated in the axial direction of the torch. Raw voltage waveforms at the
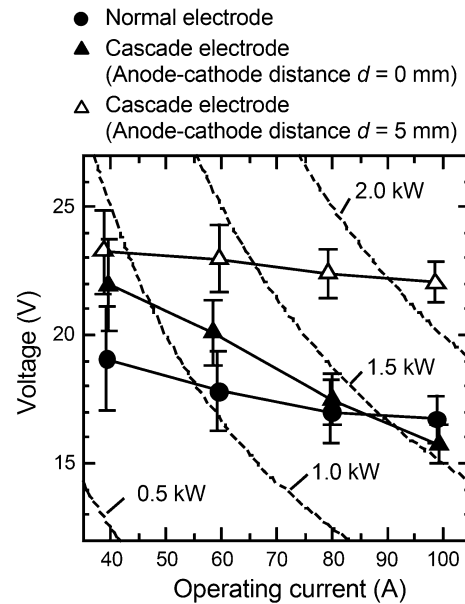
Fig. 3 Voltage–current characteristics of the cascade plasma torch for a gas flow rate of 20 L/min and anode width of 3 mm (without an external magnetic field)

Fig. 4 Voltage waveforms at an operating current of 100 A (without an external magnetic field)

Table 1 Experimental conditions

Working gas	Argon
Operating current, A	40, 60, 80, 100, 120, 160
Gas flow rate, L/min	10, 20, 30, 40
Anode–cathode distance, mm	0, 5, 10
Anode width, mm	1, 3
Recording time, ms	100
Exposure time, μs	0.2
Frame rate, fps	100,000
Image resolution, pixels	192 × 200

operating current of 100 A are shown in Fig. 4. It can be seen that the amplitude of the voltage fluctuations in the case using cascade electrode is smaller compared with that of using normal electrode. The result indicates that using cascade electrode is an effective method to reduce voltage fluctuations. It is inferred that the arc root movement in the flow direction is limited by the ring-shaped anode, thereby suppressing the arc fluctuations.

Figure 5 shows the voltage–current characteristic of the cascade plasma torch with and without the external magnetic field. The anode–cathode distance was set to 5 mm, while the other operating conditions remained the same as in the aforementioned experiment. It is seen from Fig. 5 that applying the external magnetic field tends to increase the time-averaged voltage. This can be attributed to the increase in arc resistance caused by arc rotation. When the arc rotates on the anode, heat transfer from the hot arc to the surrounding cool gas and water-cooled anode is enhanced. This enhancement is expected to reduce the arc temperature and electrical conductivity, leading to higher arc resistance and measured voltage. As a result, under the same operating current conditions, power input into the plasma torch is also increased by applying the external magnetic field. At the operating current of 100 A, the voltage increment can be seen most clearly. It can be inferred that with increasing operating current, stronger Lorentz force promotes the arc rotation which enhances heat transfer from the arc to surroundings. Figure 6 shows the comparison of the voltage waveforms with and without the external magnetic field at the operating current of 100 A. It can be seen that the amplitude of the voltage fluctuations increases by applying the external magnetic field. No clear effect of the external magnetic field on
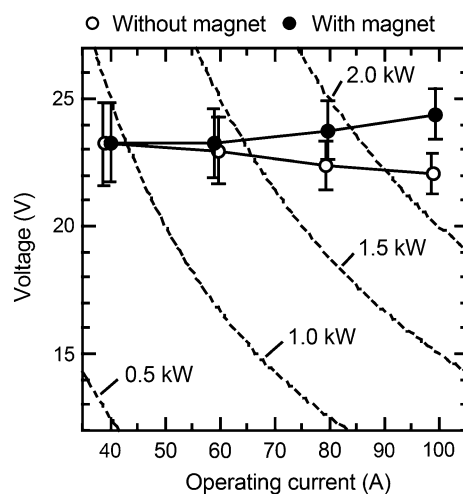
suppressing voltage fluctuations is recognized in this experimental condition.

Effects of Anode Width on Voltage Fluctuations

Figure 7 shows the end-on images of plasma jets (Fig. 7a) and voltage waveforms (Fig. 7b) for an operating current of 40 A, gas flow rate of 30 L/min, anode–cathode distance of 0 mm, and anode width of 1 mm. Each of the end-on images was originally captured as monochrome data with an 8-bit depth (256 level). These data were converted to the color scale, in which a red color represents the area of high light intensity from the plasma jets. The white solid circles represent the inner anode wall. The starting time of the measurement was taken as 0 ms. As shown in Fig. 7(a), an area with high light intensity is seen at the central part where the plasma jets are heated and accelerated by the current concentration on the cathode tip. The Lorentz force produced by the interaction between the arc current and external magnetic field drives the anode arc to rotate in the counterclockwise direction along the anode wall with no observable breakdown behavior. The voltage, which was synchronously measured with the end-on images, is presented in Fig. 7(b). The voltage waveforms show a periodic behavior according to the rotational movement of the anode arc. This periodic voltage modulation can be explained by a deviation from the ideal concentricity between the anode and cathode. The voltage takes the minimum value at approximately 3.70 ms and 4.30 ms when the anode arc rotates along the upper side of the anode wall, and it takes the maximum peak value during the arc rotation along the lower side. From this tendency, it may be inferred that the center of the cathode tip was off to the upper side from the ideal anode center and the periodic voltage modulation was caused by the variation in the length of the rotational arc.
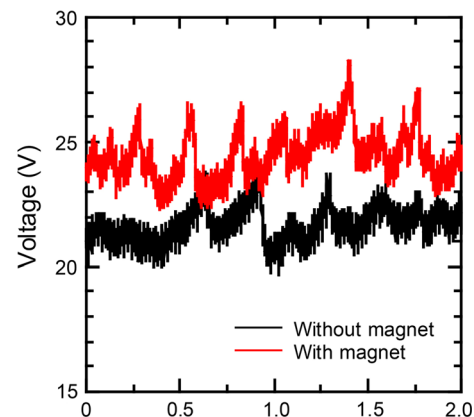

Fig. 5 Effect of the external magnetic field on the voltage–current characteristics of the cascade plasma torch for a gas flow rate of 20 L/min, anode width of 3 mm, and anode–cathode distance of 5 mm
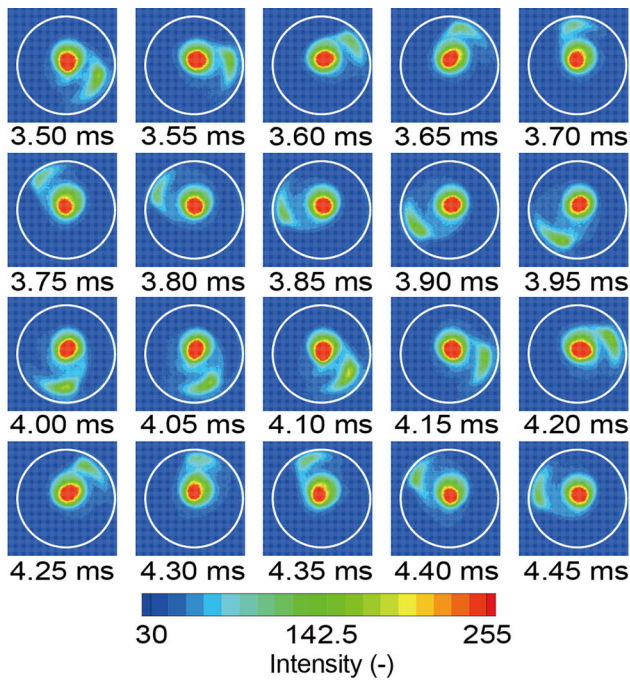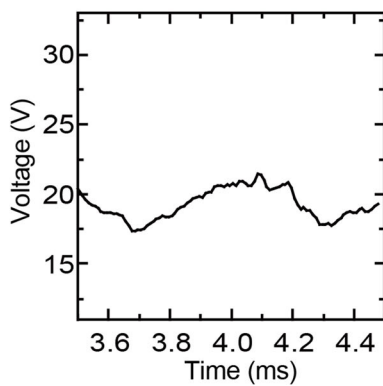

Fig. 6 Voltage waveforms with and without the external magnetic field at an operating current of 100 A
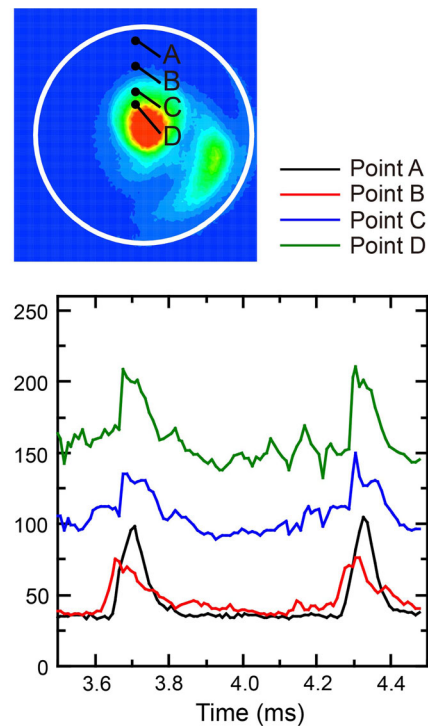
(a)

(b)

Fig. 7 (a) End-on images of plasma jets and (b) voltage waveforms for an operating current of 40 A, gas flow rate of 30 L/min, anode–cathode distance of 0 mm, and anode width of 1 mm

Fig. 8 Time variation of light intensity at several fixed points for an operating current of 40 A, gas flow rate of 30 L/min, anode–cathode distance of 0 mm, and anode width of 1 mm

The temporal variations of the light intensity corresponding to Fig. 7 at several fixed points are shown in Fig. 8. The observation point A is positioned near the upper side of the anode wall. The points B, C, and D are placed in such a manner that they gradually approach the central part of the rotational arc. The peaks of the light intensity for each observation point represent the arc passing through the points. The periodic peaks are observed for every observation point, which indicates that an arc between the anode and cathode rotates continuously on the anode wall. There is no breakdown or arc-root jump process. The magnitude of the light intensity tends to increase on approaching the central part of the rotational arc, except in the case of points A and B. This should be attributed to the concentration of current near the anode wall.
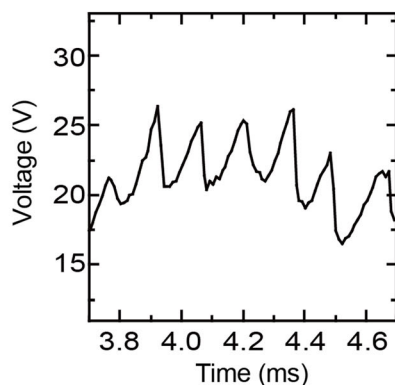
Figure 9 shows the end-on images of the plasma jets (Fig. 9a) and voltage waveforms (Fig. 9b) using the 3-mm-wide anode. The other operating conditions were set to be identical to the preceding experiment shown in Fig. 7 and 8. No continuous arc rotation is observed due to the intermittent breakdown process where the arc root suddenly jumps from one spot to another spot. For example, from 3.80 to 3.90 ms, it seems that the anode arc root rotates counterclockwise and the voltage rises during the rotational period. However, at 3.95 ms, the breakdown occurs, and multiple arcs are observed. At this moment, the voltage drops steeply. At 4.00 ms, the new anode arc root starts to rotate again. The breakdown occurs with an interval of approximately 0.1-0.15 ms as shown in Fig. 9(b). This interval has almost the same order with that of breakdown which is observed in our experiment when a normal plasma torch is used without an external magnetic field. Therefore, it can be inferred that the regularity of the breakdown interval comes from a typical breakdown process caused by the interaction between the fluid and electromagnetic field. Compared with the results shown in Fig. 7(b), more voltage fluctuations can be seen due to the repeated breakdowns.

The temporal variations of the light intensity corresponding to Fig. 9 at several fixed points are shown in Fig. 10. Point A is positioned near the center of the plasma jets, and points B to E are positioned to approach the anode
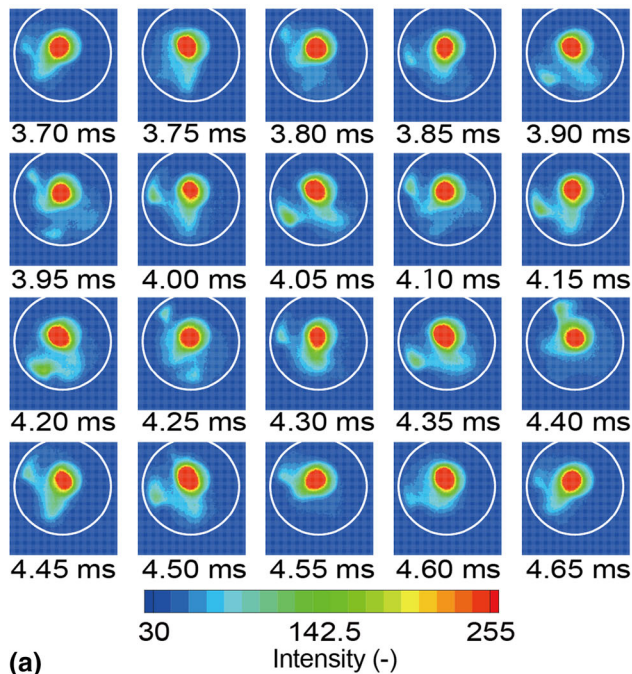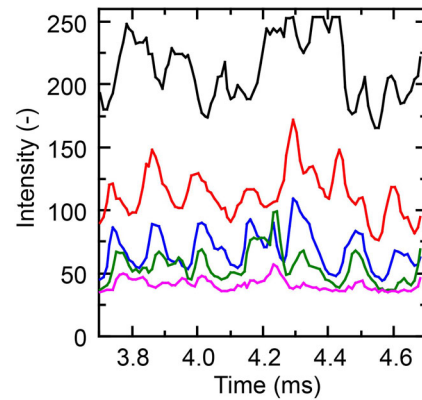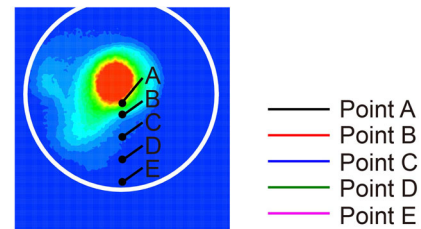
(a)

(b)

Fig. 9 (a) End-on images of plasma jets and (b) voltage waveforms for an operating current of 40 A, gas flow rate of 30 L/min, anode–cathode distance of 0 mm, and anode width of 3 mm

Fig. 10 Time variation of light intensity at several fixed points for an operating current of 40 A, gas flow rate of 30 L/min, anode–cathode distance of 0 mm, and anode width of 3 mm

use of the anode with 3 mm width is insufficient for limiting the arc root movement. For suppressing the arc chaotic fluctuations and promoting the continuous arc rotation, the anode with 1 mm width performs better. It should be noted that the narrow ring-shaped anode is expected to be severely damaged at high operating current condition that exceeds 100 A due to its low heat capacity. The anode cooling technique is important factor for high-power operation.

Effects of Gas Flow Rate on Voltage Fluctuations

The anode of 1 mm width was used in the experiment. The operating current, gas flow rate, and anode–cathode distance were set to 40 A, 10 L/min, and 0 mm, respectively. It is clearly seen from Fig. 11(a) that the anode arc root rotates continuously without breakdown. The voltage shows periodic sine-like fluctuations corresponding to the rotational movement of the anode arc root. One possible explanation for the periodic voltage fluctuations is that the cathode center is displaced from the center of the anode wall. In the experiment, a commercial rod-type cathode and cathode-surrounding ceramic nozzle, originally for plasma welding, were used. There is some inherent variation in its dimension, and it is difficult to match the cathode center with the center of the anode wall exactly. From the end-on images, the cathode center seems closer to the upper side of the anode wall than the lower side, resulting in the temporal variation of arc length during the arc rotation. The

wall. It is found that the light intensity tends to increase as the point positions progress from the anode wall to the center of the plasma jets. At point A, the measured light intensity is saturated at approximately 4.30 ms. The light intensity waveforms for each point appear to be strongly correlated, and at the points B, C, and D, it can be seen clearly that the peaks of the light intensity fluctuations correspond to those of the measured voltage shown in Fig. 9(b). This is because the repeated arc jumps by breakdown occur at the lower side of the anode in which there are the fixed measurement points of the light intensity. However, it should be noted that in our experiment, the points where the arc jumps were irregularly changed during the operation. From the results shown in Fig. 7 and 9, it is inferred that the trigger for the breakdown process comes from the arc movement in the flow direction, and the
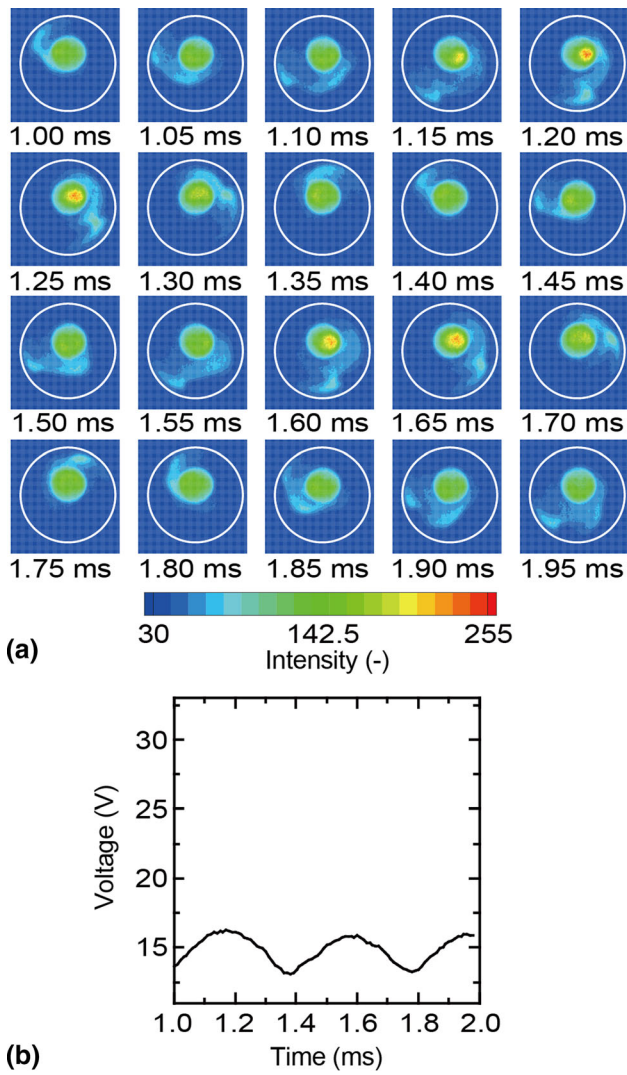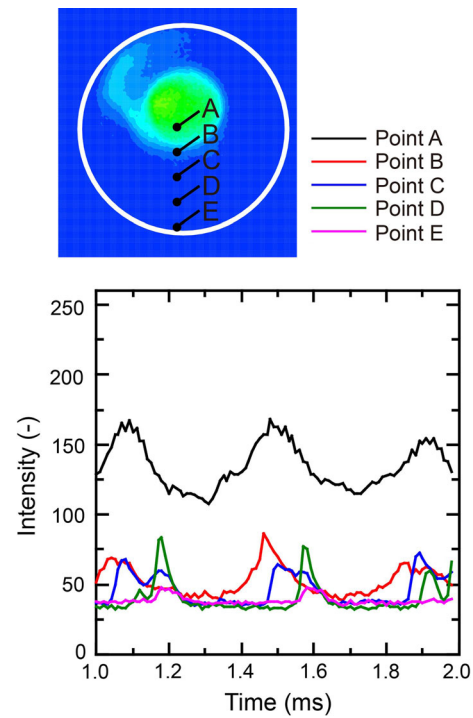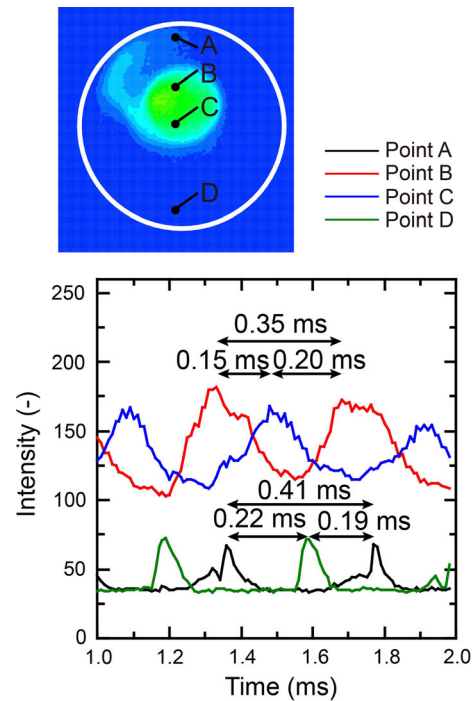
(a)

(b)

Fig. 11 (a) End-on images of plasma jets and (b) voltage waveforms for an operating current of 40 A, gas flow rate of 10 L/min, anode–cathode distance of 0 mm, and anode width of 1 mm

voltage reaches its peak when the arc root slides along the lower side of the anode wall at approximately 1.20 ms and 1.60 ms. It reaches the minimum value when the arc root slides along the upper side at approximately 1.35 ms and 1.75 ms.

Figure 12 shows the temporal variations of light intensity corresponding to Fig. 11 at the fixed observation points designated as A to E. The point A is positioned near the center of the plasma jets, and the points B to E are positioned such that they gradually approach the anode wall. The periodic peaks are observed for each point and represent the passing of the rotational arc. As we approach the center of the plasma jets, a higher light intensity is measured except between points C and D. This should be

Fig. 12 Time variation of light intensity at several fixed points for an operating current of 40 A, gas flow rate of 10 L/min, anode–cathode distance of 0 mm, and anode width of 1 mm
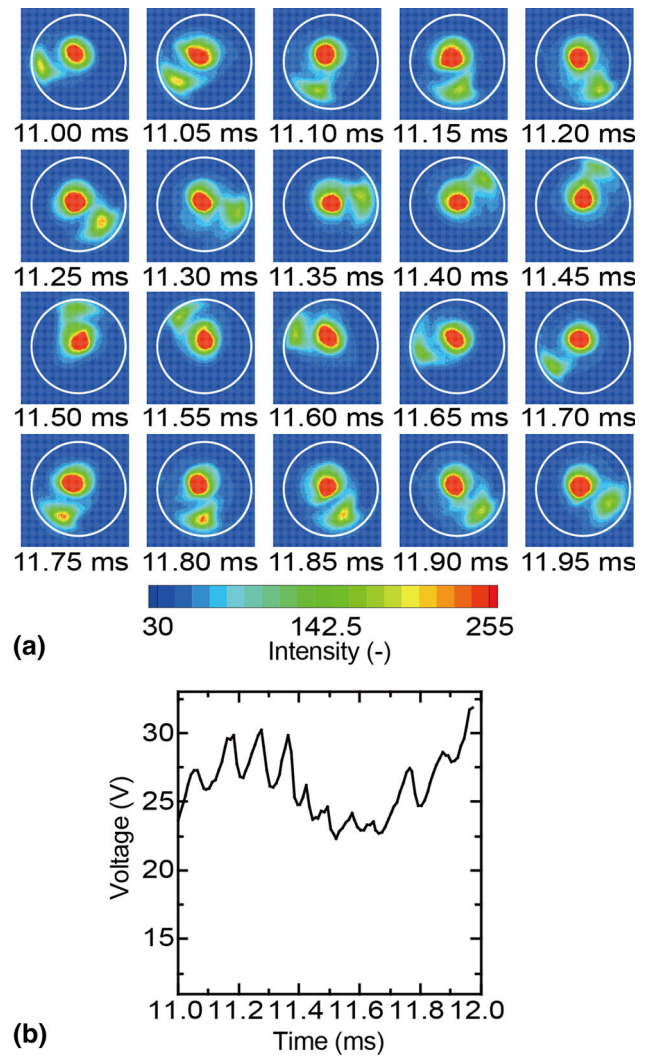

Fig. 13 Arc rotation period of the central and near-anode wall region for an operating current of 40 A, gas flow rate of 10 L/min, anode–cathode distance of 0 mm, and anode width of 1 mm

attributed to the current concentration near the anode wall. In addition, it is found that the peaks of the light intensity come early at the points A–C compared with the points D and E. This indicates that the arc has a spiral structure during the rotation.

Figure 13 shows the arc rotation period of the central and near-anode wall region. The points A and D are fixed points near anode wall, positioned opposite to each other. The alternate peaks of the light intensity are observed for points A and D by the arc root rotation along the anode wall. The intervals from the peak at the point A to D and D to A correspond to the period of arc rotation along the anode wall at the left side and right side, respectively. It is found that the period for the left-side rotation is approximately 0.22 ms, which is longer than that for the right-side rotation of approximately 0.19 ms. The alternate peaks are also observed at points B and C, positioned in the central region of the plasma jets. The period of the arc rotation for the left side, however, is shorter than that for the right side, which is 0.15 ms and 0.20 ms, respectively. These differences in the rotation period for the left and right sides indicate that the arc is elongated during the left-side rotation, while it contracts during the right-side rotation. When the arc rotates on the left side, the angular velocity of the arc root is lower than that of the center region of the arc as shown in Fig. 11(a) from 1.00 to 1.15 ms. It is inferred that the arc root is affected by wall friction, and the difference of the angular velocity between the arc root and center region results in the elongation of the arc length. At 1.20 ms, the light intensity of the anode arc root increases. This means that the concentration of electric current density occurs through the arc elongation. Therefore, stronger Lorentz force accelerates the anode arc root, leading to the arc contraction during the right-side rotation. This repetitive elongation and contraction behavior leads to the periodic voltage waveforms shown in Fig. 11(b).

Figure 14 shows the end-on images of the plasma jets (Fig. 14a) and voltage waveforms (Fig. 14b) at a gas flow rate of 40 L/min. The other operating conditions are the same as the preceding experiment shown in Fig. 11, 12 and 13. Continuous rotation of the anode arc root is observed, and the measured voltage tends to become high when the anode arc root rotates on the lower side of the anode wall and low when the rotation is on the opposite side. The voltage waveforms, however, include some fluctuations during the arc rotation cycle. The time variations of the light intensity corresponding to Fig. 14 at the fixed observation points are shown in Fig. 15. The observation point A is positioned near the center of the plasma jets, and the points B to D are positioned such that they approach the anode wall. The light intensity measured at the points C and D, which are points near the anode wall, shows the periodic peaks that correspond to the passing of the arc
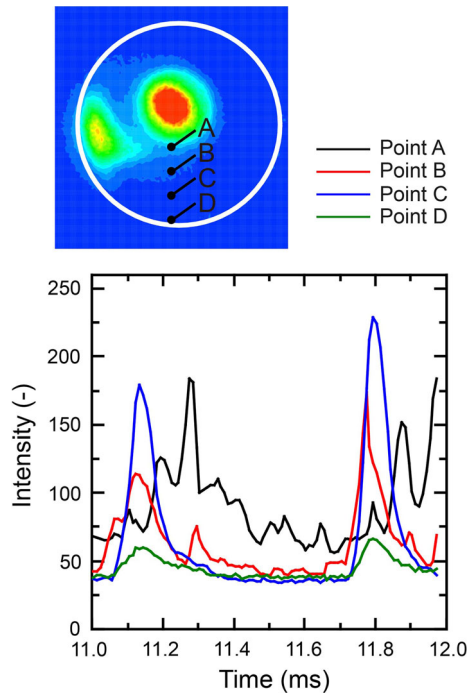

Fig. 14 (a) End-on images of plasma jets and (b) voltage waveforms for an operating current of 40 A, gas flow rate of 40 L/min, anode–cathode distance of 0 mm, and anode width of 1 mm

root. The light intensity at the point A, however, exhibits a chaotic behavior. These results indicate that a high gas flow rate tends to cause voltage fluctuations in the cascade plasma torch with an external magnetic field and hamper the continuous arc rotation.

Effects of Operating Current on Arc Rotational Frequency

Figure 16 shows the raw voltage waveforms (Fig. 16a) and voltage–power spectra (Fig. 16b) for different operating currents. The gas flow rate, anode–cathode distance, and anode width were set to 10 L/min, 0 mm, and 1 mm, respectively. As presented in Fig. 16(a), the voltage waveforms exhibit a periodic behavior which corresponds to the rotational movement of the arc for each operating current condition, and some instability is introduced at

Fig. 15 Time variation of light intensity at several fixed points for an operating current of 40 A, gas flow rate of 40 L/min, anode–cathode distance of 0 mm, and anode width of 1 mm

160 A. The strength of the voltage amplitudes indicates no trend for the operating currents. More detailed experimental and numerical efforts are needed to elucidate this

physical phenomenon since the experimental data of the voltage measurement and high-speed photography were insufficient to explain this relation between the voltage amplitude and operating current. The power spectra obtained by the FFT analysis are shown in Fig. 16(b). It can be seen clearly that the peaks corresponding to the arc rotation are dominant and their frequencies rise with increasing operating current. If it is assumed that the Lorentz force and drag force are balanced for the rotational arc, the following equation is generally accepted as a rough approximation (Ref 18):

$$IBd = \frac{1}{2} C_d D \rho V^2 d \qquad \text{(Eq 1)}$$

where I is the arc current, B is the magnetic flux density, D is a dimension normal to the direction of motion, V is the arc velocity, C_d is the drag coefficient, ρ is the gas density, and d is the distance between the electrodes. From Eq 1, it is found that the arc rotational velocity is proportional to the square root of the operating current, and it is also expected that the arc rotational velocity is strongly correlated with the arc rotational frequency. Figure 17 shows the variation of the peak frequency with operating current. The peak frequencies are proportional to the square root of the operating current, and the constant of proportionality is approximately 0.4 in our experiment. From this result, the assumption of Eq 1 is valid enough when continuous arc rotation without observable breakdowns occurs in the range
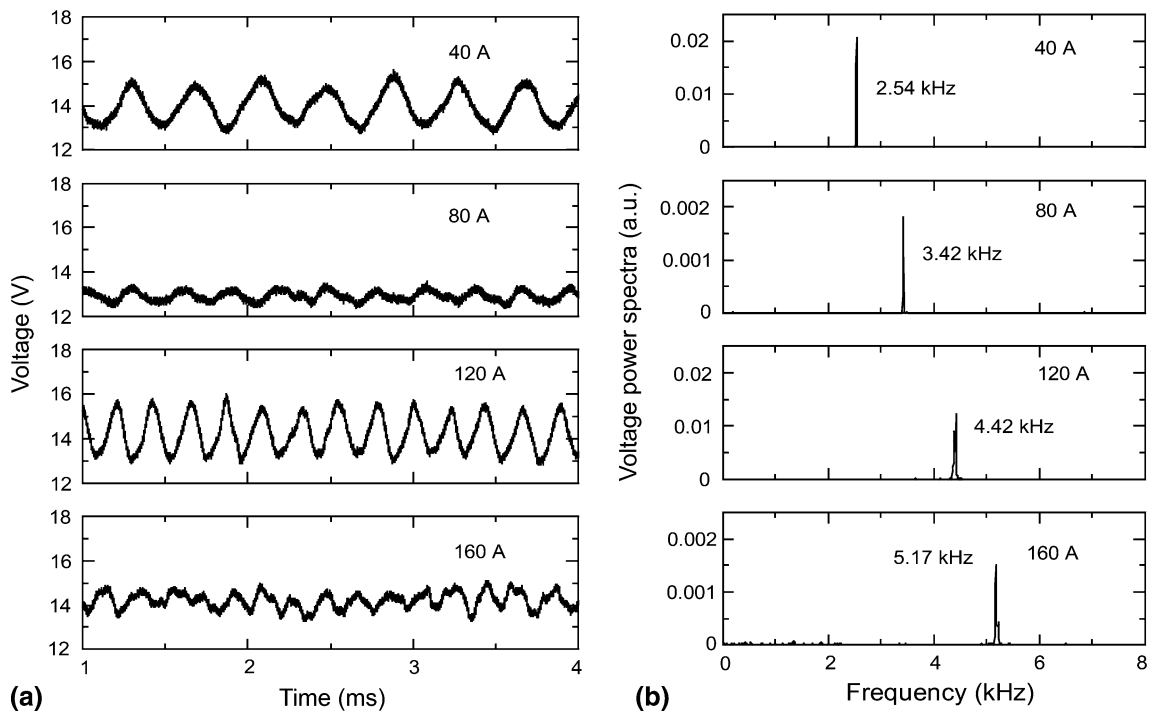
Fig. 16 (a) Voltage waveforms and (b) voltage–power spectra for different operating currents for a gas flow rate of 10 L/min, anode–cathode distance of 0 mm, and anode width of 1 mm

$$f_{peak} \approx 0.4\, I^{1/2}$$
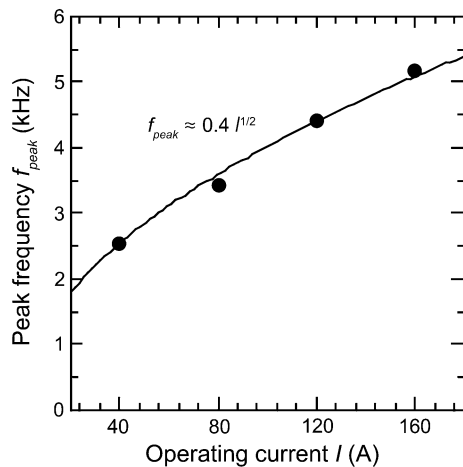
Fig. 17 Variation of arc rotational frequency with operating current

below approximately 160 A. This fact would be useful information for predicting or modeling the plasma process in a cascade plasma torch with an external magnetic field.

Although the power of the experimental plasma torch was small compared with that of a practical plasma torch for thermal spraying, the results obtained in this work will probably help the formation of approaches to the development of a plasma torch with low power fluctuations. Higher-voltage operation by increasing the anode–cathode distance would be desirable for scaling up the torch power because high operating current may severely damage the ring-shaped anode. To raise operating voltage of the experimental plasma torch, a pilot arc circuit for plasma ignition is expected to be effective, which enables an arc discharge for a longer anode–cathode distance (Ref 12). The strength of the external magnetic field, which was not varied in our experiment, would also be a key factor for generating plasma jets with low power fluctuations because Lorentz force is inferred to affect an amplitude of voltage fluctuations as shown in Fig. 16. Besides, the effects of the swirl flow generated by the rotating arc on the sprayed particles and coating structures may be a subject of further investigation. More detailed study should be necessary to decide the strength of the external magnetic field which is appropriate for thermal spraying process.

Conclusions

Voltage measurement and high-speed photography were conducted for a cascade plasma torch in the presence of an external magnetic field. The effects of using a cascade electrode and applying an external magnetic field on the voltage–current characteristics were also studied. The time-averaged arc voltage showed a positive trend with the increase in the anode–cathode distance, and a higher time-averaged voltage was obtained by applying an external magnetic field. The results of the high-speed photography showed that the narrow ring-type anode and the low gas flow rate were key factors that lead to the low voltage fluctuations caused by the arc breakdown process. In the experiment, periodic sine-like voltage waveforms were obtained under the operating condition using the anode of 1 mm width at a gas flow rate of 10 L/min. The periodic voltage fluctuations should be attributed to the periodic elongation and contraction of the rotational arc by the displacement between the cathode tip and the axis of the plasma torch nozzle. The periodic behavior of the voltage waveforms is expected to improve the controllability of the input power into plasma jets as the input power is always controlled in the range of the voltage wave amplitude without the occurrence of any irregular voltage fluctuations. The estimated frequencies of the arc rotation were over 1 kHz and tended to be proportional to the square root of the operating currents. Our further efforts will be focused on upscaling the torch power and examining whether this periodic behavior works to improve the controllability of the heat and momentum transfer to the sprayed particles.

References

1. V. Rat, F. Mavier, and J.F. Coudert, Electric Arc Fluctuations in DC Plasma Spray Torch, *Plasma Chem. Plasma Process.*, 2017, **37**(3), p 549-580
2. J.F. Coudert, M.P. Planch, and P. Fauchais, Velocity Measurements of DC Plasma Jets Based on Arc Root Fluctuations, *Plasma Chem. Plasma Process.*, 1995, **15**(1), p 47-70
3. J.R. Fincke, D.M. Crawford, S.C. Snyder, W.D. Swank, D.C. Haggard, and R.L. Williamson, Entrainment in High-velocity, High-temperature Plasma Jets. Part I: Experimental Results, *Int. J. Heat Mass Transf.*, 2003, **46**(22), p 4201-4213
4. R.L. Williamson, J.R. Fincke, D.M. Crawford, S.C. Snyder, W.D. Swank, and D.C. Haggard, Entrainment in High-velocity, High-temperature Plasma Jets: Part II: Computational Results and Comparison to Experiment, *Int. J. Heat Mass Transf.*, 2003, **46**(22), p 4215-4228
5. J. Hlína and J. Šonký, Time-Resolved Tomographic Measurements of Temperatures in a Thermal Plasma Jet, *J. Phys. D Appl. Phys.*, 2010, **43**(5), p 055202
6. J.F. Bisson, B. Gauthier, and C. Moreau, Effect of Plasma Fluctuations on In-flight Particle Parameters, *J. Therm. Spray Technol.*, 2003, **12**(1), p 38-43
7. J.F. Bisson and C. Moreau, Effect of Direct-Current Plasma Fluctuations on In-flight Particle Parameters: Part II, *J. Therm. Spray Technol.*, 2003, **12**(2), p 258-264
8. S.A. Wutzke, E. Pfender, and E.R.G. Eckert, Study of Electric-Arc Behavior with Superimposed Flow, *AIAA J.*, 1967, **5**(4), p 707-714

9. S.A. Wutzke, E. Pfender, and E.R.G. Eckert, Symptomatic Behavior of an Electric Arc with a Superimposed flow, *AIAA J.*, 1968, **6**(8), p 1474-1482

10. Z. Duan and J. Heberlein, Arc Instabilities in a Plasma Spray Torch, *J. Therm. Spray Technol.*, 2002, **11**(1), p 44-51

11. M.F. Zhukov and I.M. Zasypkin, *Brief Description of Thermal Plasma and Electric Heating of Gas, Thermal Plasma Torches*, Cambridge International Science Publishing, Cambridge, 2007

12. O.P. Solonenko and A.V. Smirnov, Advanced Oxide Powders Processing Based on Cascade Plasma, *J. Phys: Conf. Ser.*, 2014, **550**, p 012017

13. https://www.oerlikon.com/metco/en/products-services/coating-equipment/thermal-spray/spray-guns/coating-equipment-plasma/triplexpro-210. Accessed 28 June 2019

14. P.L. Fauchais, J.V.R. Heberlein, and M.I. Boulos, *DC Plasma Spraying, Thermal Spray Fundamentals*, Springer, Berlin, 2014

15. M.F. Zhukov and I.M. Zasypkin, *Direct Current Linear Plasma Torches, Thermal Plasma Torches*, Cambridge International Science Publishing, Cambridge, 2007

16. L.C. Li, W.D. Xia, H.L. Zhou, Z.P. Zhou, and B. Bai, Experimental Observation and Numerical Analysis of Arc Plasmas Diffused by Magnetism, *Eur. Phys. J. D*, 2008, **47**(1), p 75-81

17. M. Hu, S. Wan, Y. Xia, Z. Ren, and H. Wang, Effect of an External Magnetic Field on Plasma Torch Discharge Fluctuation, *EPL*, 2013, **102**(5), p 55002

18. R.N. Szente, R.J. Munz, and M.G. Drouet, Arc Velocity and Cathode Erosion Rate in a Magnetically Driven Arc Burning in Nitrogen, *J. Phys. D Appl. Phys.*, 1988, **21**(6), p 909-913

19. V. Goyal, G. Ravi, P. Bandyopadhyay, S. Banerjee, V. Yugesh, and S. Mukherjee, Study of Dynamical Behaviour of the Plasma in a DC Non-transferred Plasma Torch Using Fast Imaging, *Phys. Plasmas*, 2017, **24**(3), p 033506

20. C. Wang, Z. Lu, D. Li, W. Xia, and W. Xia, Effect of the Magnetic Field on the Magnetically Stabilized Gliding Arc Discharge and Its Application in the Preparation of Carbon Black Nanoparticles, *Plasma Chem. Plasma Process.*, 2018, **38**(6), p 1223-1238

21. https://www.neomag.jp/mag_navi/gausscal/gauss_form_cylinder.php?ctype=1&magtype=1&gradename = 3&Br = 12700. Accessed 28 June 2019